Advances in Engineering Software 173 (2022) 103241

Contents lists available at ScienceDirect

Advances in Engineering Software

journal homepage: www.elsevier.com/locate/advengsoft

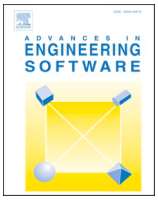

Solution of the generalized eigenvalue problem using overlapping finite elements

Sungkwon Lee, Klaus-Jürgen Bathe *

Department of Mechanical Engineering, Massachusetts Institute of Technology, Cambridge, MA 02139, USA

ARTICLE INFO

Keywords:
Overlapping finite elements and AMORE
Generalized eigenvalue problem
Frequencies and mode shapes
Mode superposition
Accuracy and convergence
Computational effort

ABSTRACT

Our objective in this paper is to present the use of the overlapping finite elements and the AMORE scheme for the solution of the generalized eigenvalue problem of solids and structures – to calculate frequencies and mode shapes – and the solution of dynamic response by mode superposition. For the solution of eigenvalues and vectors, we use the enriched subspace iteration scheme. We focus on the differences in use that arise when employing the overlapping finite elements versus traditional finite elements and the convergence of the eigenvalues and vectors as the mesh is refined. Our studies show that the use of the overlapping finite elements for frequency and dynamic solutions can be quite effective.

1. Introduction

The analysis of a structure, already built or in design, frequently requires the solution of structural dynamics problems. These solutions then often involve free vibration analyses giving the natural frequencies and mode shapes of the structure. The natural frequencies and mode shapes are fundamental characteristics to identify dynamic behavior like resonance, which may lead to structural failure, and the mode shapes are used in a mode superposition solution of structural response. Also, a vibration analysis can be employed for assessing the quality of a discretization for further dynamic analyses and the proper time step selection for a direct integration of transient response [1].

In engineering practice, the use of low order finite elements is often preferred in static and dynamic analyses. Low order finite elements are computationally inexpensive but prone to loss of accuracy due to mesh distortions, and the predicted stresses can be poor unless the mesh is sufficiently fine [1–3]. These observations hold also for the 4-node incompatible mode element for two-dimensional analyses and the 8-node incompatible mode element for three-dimensional analyses. We additionally note that higher order elements like the 8-node quadrilateral element for two-dimensional solutions can show poor predictive capabilities when distorted elements are used [1,4].

The overlapping finite element (OFE) method we have studied shows good predictive capabilities even when the mesh is distorted and relatively coarse [2,5–10]. Our experience in using the OFE method in static analysis is that compared with the (traditional) finite element method, the solution usually requires a coarser mesh to reach the same solution accuracy. Also, as in the finite element method, the numerical integration can be effectively performed using the usual Gaussian quadrature when polynomial bases are used. The overlapping finite element discretization is also effective for the solution of wave propagation problems [11–13]. The discretization enables a more accurate solution than using the traditional finite element method, and the solution accuracy achieved is quite insensitive to the propagation direction. Given these promising observations, we explore in this paper the use of overlapping finite elements for free vibration and mode superposition analyses.

The overlapping finite element method is closely related to various approaches using enrichment techniques. In Refs. [14,15] a generalized finite element method is proposed. The initially discussed method was shown to be unstable with polynomial enrichments, and procedures to reach stability were introduced. Special solvers for the positive semi-definite matrix were used in the early development [14,15], and more recently an enrichment modification was suggested [16]. The enrichment modification achieves stability when proper partition of unity functions are used. Higher order polynomial enrichments with the enrichment modification are studied in Refs. [17,18] showing the use of the flat-top partition of unity function to achieve stability. Another approach for stable polynomial enrichments is the use of the piecewise-linear partition of unity function [19,20]. These non-smooth partition of unity functions [17–20] can be useful to reach stability but introduce stress jumps *within* the elements, these jumps are undesirable in solving many practical problems. Enrichment techniques are

* Corresponding author.
E-mail address: kjb@mit.edu (K.J. Bathe).

https://doi.org/10.1016/j.advengsoft.2022.103241
Received 16 June 2022; Received in revised form 22 July 2022; Accepted 23 July 2022
Available online 22 September 2022

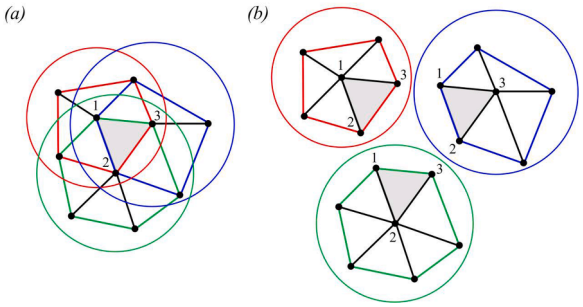

Fig. 1. (a) A triangular overlapping finite element with nodes 1, 2, and 3; (b) the overlapping finite element corresponds to the overlapped region of the three polygonal elements associated with each node of the overlapping element; the circles indicate the corresponding finite spheres for the overlapping finite element [5,6,27].

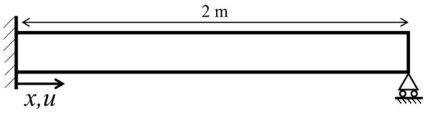

Fig. 2. Frequency analysis of a one-dimensional rod; Young's modulus = 200 GPa, density = 7800 kg/m^3, and the cross-sectional area = 0.2 m^2.

also used for the solution of the natural frequencies and then often with non-polynomial enrichments [21–23]. The advantages of the overlapping finite elements are smooth stress predictions within the elements, an insensitivity to element geometric distortions, and numerical stability. Although we only consider the use of polynomial bases in this work, we note that our overlapping finite element discretization can also adopt other enrichment functions, e.g., see Refs. [11–13].

In this paper, we use the overlapping finite element formulation introduced in Refs. [9,10] for free vibration and mode superposition analyses. The Bathe enriched subspace iteration method [24] is utilized to calculate the frequencies and mode shapes, see Ref. [25] for the source code of the method. Considering solution times, we optimize the equation ordering using the reverse Cuthill-McKee algorithm [26] but do not report this time used. We measure and report in the paper the CPU time used to establish the stiffness and mass matrices and the solution by the subspace iteration procedure and time integration.

In the following section, the overlapping finite element discretization is briefly reviewed and discussed in comparison with the traditional finite element discretization. In Section 3, the basic theory for the solution of frequencies and mode shapes and also the method of mode superposition are presented with a view towards the use of the overlapping finite element method. In Section 4, we provide numerical examples showing the characteristics and effectiveness of the method. Lastly, we give our concluding remarks in Section 5.

2. The overlapping finite element method

The overlapping finite element method gives the global field by interpolating the local fields of the polygonal elements that overlap each other

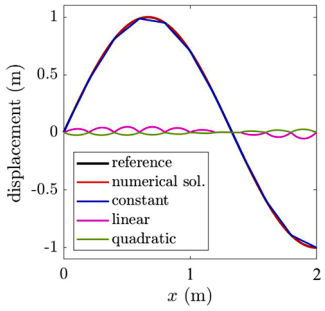

Fig. 4. The second mode shape obtained using the quadratic overlapping element; the numerical solution is the sum of the displacements given by the constant, linear, and quadratic terms; the displacement shown is in the longitudinal x-direction.

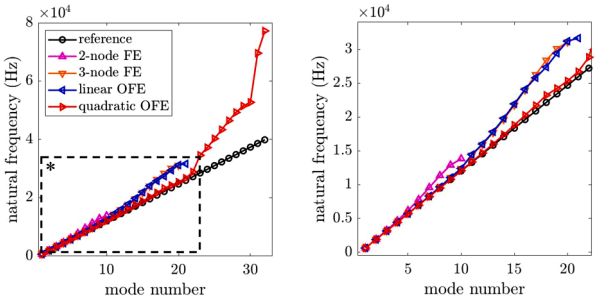

Fig. 3. The natural frequencies of the one-dimensional bar calculated using traditional finite elements and overlapping finite elements; the right figure corresponds to the box labeled with an asterisk in the left figure.

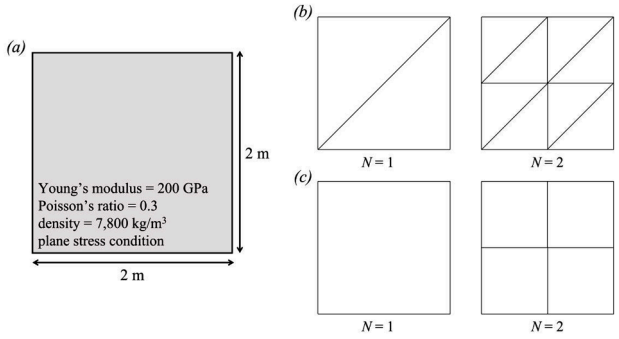

Fig. 5. Free vibration analysis of an unsupported plate for in-plane vibrations; (a) Description of the problem; (b) Meshes using triangular elements; (c) Meshes using quadrilateral elements; N is the number of elements per side of the analysis domain, and we consider the use of $N = 1$, 2, 4, 8, and 16.

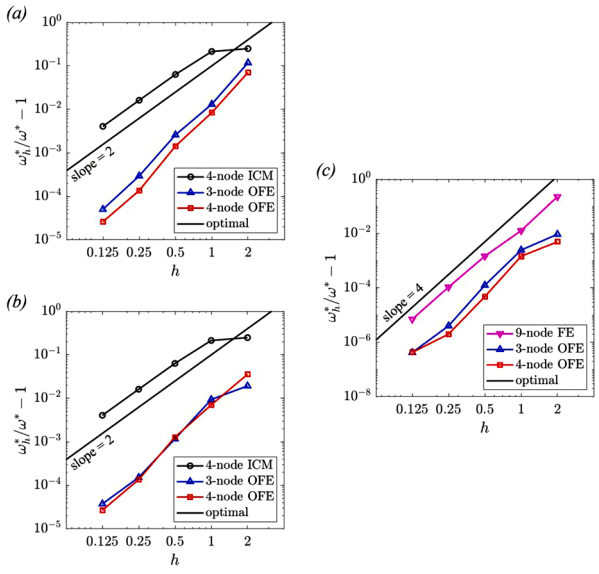

Fig. 6. Convergence studies with two-dimensional overlapping elements; h = size of element (i.e., $2/N$); the ω_h^* and ω^* represent the numerical and reference solutions of the smallest nonzero frequency, respectively; (a) use of linear basis; (b) bilinear basis; (c) quadratic basis; the labels '4-node ICM' and '9-node FE' indicate the use of the incompatible mode element and the traditional 9-node finite element, respectively.

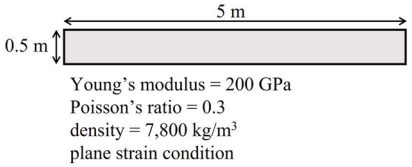

Fig. 7. A two-dimensional free-free beam.

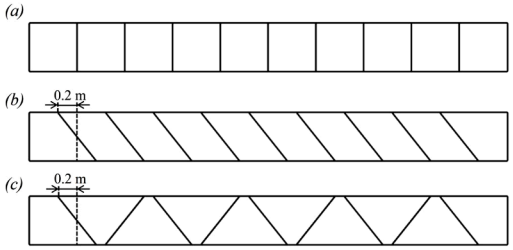

Fig. 8. The meshes used for the frequency analysis of the free-free beam; (a) The mesh without distortion; (b) The mesh with parallelogram distortion; (c) The mesh with trapezoidal distortion.

$$u = \sum_I h_I \psi_I \tag{1}$$

where u is the global scalar field to be calculated, h_I is the low order finite element function for node I of the overlapping element, and ψ_I is the local field given by the polygonal element associated with node I, see Fig. 1.

Following the technique used in the method of finite spheres [27] (see the spheres in Fig. 1), the local field of each polygonal element is constructed by interpolating nodal functions

$$\psi_I = \sum_K \phi_K^I u_K \tag{2}$$

Table 1
The five smallest nonzero natural frequencies of the two-dimensional free-free beam; for the overlapping elements β = 0.01 is used.

	Reference	105.3 (Hz)	273.6	498.4	530.4	759.4
4-node linear OFE (132 dofs)	Undistorted	105.6	274.5	501.8	530.4	769.5
	Parallelogram	106.1	277.1	512.0	530.4	799.5
	Trapezoidal	106.2	278.9	517.2	530.4	808.0
4-node quadratic OFE (264 dofs)	Undistorted	105.3	273.6	498.4	530.4	759.6
	Parallelogram	105.3	273.7	498.5	530.4	760.2
	Trapezoidal	105.3	273.7	498.9	530.4	761.6
4-node ICM (44 dofs)	Undistorted	107.1	289.8	557.8	533.0	906.9
	Parallelogram	106.4	283.9	536.7	532.8	856.6
	Trapezoidal	173.5	461.7	862.7	533.6	1342.1
9-node FE (126 dofs)	Undistorted	105.6	275.8	506.2	530.4	778.6
	Parallelogram	105.8	277.7	513.7	530.4	799.0
	Trapezoidal	105.8	278.0	516.1	530.4	808.1

where ϕ_K^I fulfills the partition of unity over K and u_K is the nodal function at node K. The nodal function u_K is composed of functions with unknown coefficients. Consequently, in this method the unknowns in the algebraic governing equations are the coefficients used for defining nodal functions. We recall that, in contrast, in the traditional finite element method just nodal values are used for interpolation to build the global field.

The essential nodal functions for the overlapping finite element method are the linear polynomials because they enable the element to pass the patch test [1,2]. Considering the overlapping element in Fig. 1 and an arbitrary linear polynomial field p_L we note that using $u_1 = u_2 = u_3 = p_L$ results in the global scalar field reproducing p_L

$$u = \sum_I h_I \psi_I = \rho_1 u_1 + \rho_2 u_2 + \rho_3 u_3 = (\rho_1 + \rho_2 + \rho_3) p_L = p_L \tag{3}$$

where the ρ_K satisfy $\rho_1 + \rho_2 + \rho_3 = 1$.

For a 3-node linear overlapping finite element we define three nodal linear polynomials which require eighteen degrees of freedom in total. Compared with a 3-node finite element which requires six degrees of freedom, more degrees of freedom are used in a 3-node linear overlapping finite element. The bandwidth of the global stiffness matrix obtained using the overlapping finite element method is consequently larger than in the finite element method. However, we note that the above properties do not imply that the overlapping finite element method is computationally inefficient. In Section 4, we provide numerical examples showing the computational efficiency of solution using the overlapping finite elements.

Using the overlapping element approach in Refs. [9,10], we also have

$$\rho_K = h_K + \beta \sum_J (h_J - h_K) \widehat{h}_{JK} \tag{4}$$

where J indicates the nodes connected to node K by an edge and $\widehat{h}_{JK}$ is the standard higher order finite element function corresponding to the mid-point between nodes J and K. We have shown that the use of a small value of β (e.g., 0.01) is very effective in achieving both stability and good solution accuracy [9,10].

For example, considering the 4-node quadrilateral overlapping element with the linear polynomial basis, we see that with β a small value, the overlapping element performs almost like a quadratic element (i.e., like the 4-node finite element with linear covers [28]).

In practice, the low order finite element with incompatible modes is widely used because it performs when geometrically undistorted like a quadratic element especially in a bending-dominant problem [1]. However, the use of the incompatible mode element can be quite

Table 2
Solution of plate for smallest 10 frequencies; all times are normalized by the actual total CPU time used for the 4-node incompatible mode element (ICM) solution; note that both meshes give the relative error of 0.2% for the first frequency.

Mesh	Numerical integration time	Time for time integration	Total CPU time	Half-bandwidth of **K**	Total degrees of freedom
AMORE	8.4×10^{-2}	4.6×10^{-1}	9.7×10^{-1}	102	1502
4-node ICM	1.3×10^{-1}	4.2×10^{-1}	1.0×10^{0}	82	1622

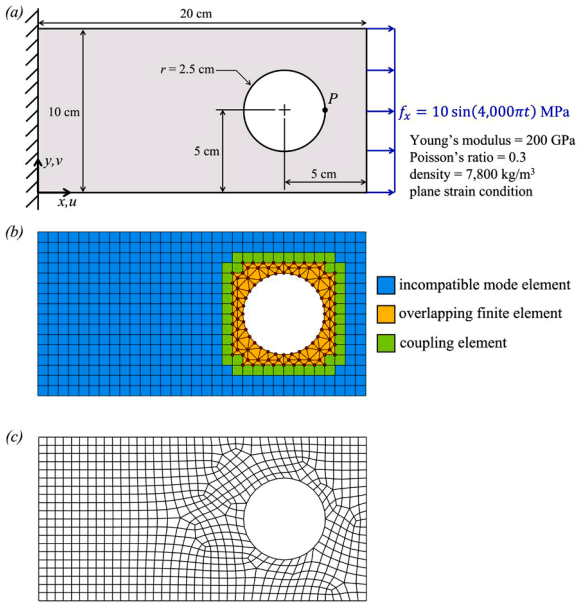

Fig. 9. Forced vibration analysis of a plate with a hole; (a) Problem description; the structure is subjected to a varying x-direction traction; t denotes the time elapsed in seconds; (b) AMORE mesh using the linear basis and β = 0.01; the red nodes are overlapping finite element nodes; (c) The traditional mesh using the 4-node incompatible mode element.

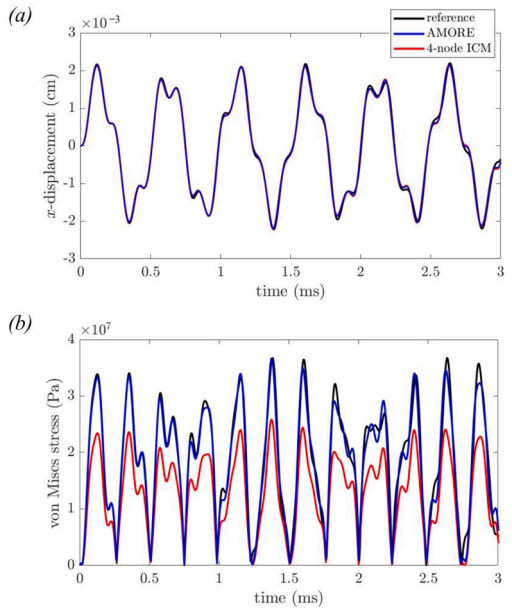

Fig. 10. Numerical predictions at point P shown in Fig. 9(a); (a) The x-displacement; (b) The von Mises stress.

ineffective when the elements are distorted [2]. Our experience is that the linear overlapping element not only performs almost like the traditional quadratic element but also is relatively insensitive to mesh distortions.

When used with polynomial bases, the shape functions of the overlapping finite element are polynomials. Therefore, we can perform the numerical integration effectively using Gaussian quadrature as in the finite element method [1]. Since the shape functions are high-order polynomials, the computational cost of the numerical integration is higher but still reasonable and, as in the standard finite element method, only a relatively small fraction of the computational cost used for the solution of the governing equations, see Section 4 for examples.

We finally note that the condition number of the global stiffness matrix given by the overlapping finite element discretization is reasonable. Our numerical experiments [9,10] show that the condition number usually lies within the range of the numbers encountered with the traditional finite element discretizations in practical analyses.

3. The free vibration and mode superposition analyses

In principle, the free vibration and mode superposition analyses using overlapping finite elements are performed as in traditional finite solutions [1]. However, some attention needs to be given to the use of the polynomial bases in the degrees of freedom.

3.1. Free vibration analysis

For the m-th overlapping finite element, we have

$$\mathbf{U}^{(m)} = \mathbf{H}^{(m)}\mathbf{a}^{(m)} \tag{5}$$

where $\mathbf{U}^{(m)}$ is the displacement vector in the Cartesian coordinate system, $\mathbf{H}^{(m)}$ is the displacement interpolation matrix, and the vector $\mathbf{a}^{(m)}$ is the unknown coefficient vector. For example, when the linear polynomial basis is used for the nodal function of a 3-node triangular overlapping element we have

$$\mathbf{H}^{(m)} = \begin{bmatrix} \mathbf{h}_1 & \mathbf{h}_2 & \mathbf{h}_3 & \mathbf{0} & \mathbf{0} & \mathbf{0} \\ \mathbf{0} & \mathbf{0} & \mathbf{0} & \mathbf{h}_1 & \mathbf{h}_2 & \mathbf{h}_3 \end{bmatrix} \tag{6}$$

$$\mathbf{a}^{(m)} = [\,\mathbf{a}_1^u \quad \mathbf{a}_2^u \quad \mathbf{a}_3^u \quad \mathbf{a}_1^v \quad \mathbf{a}_2^v \quad \mathbf{a}_3^v\,]^T$$

where

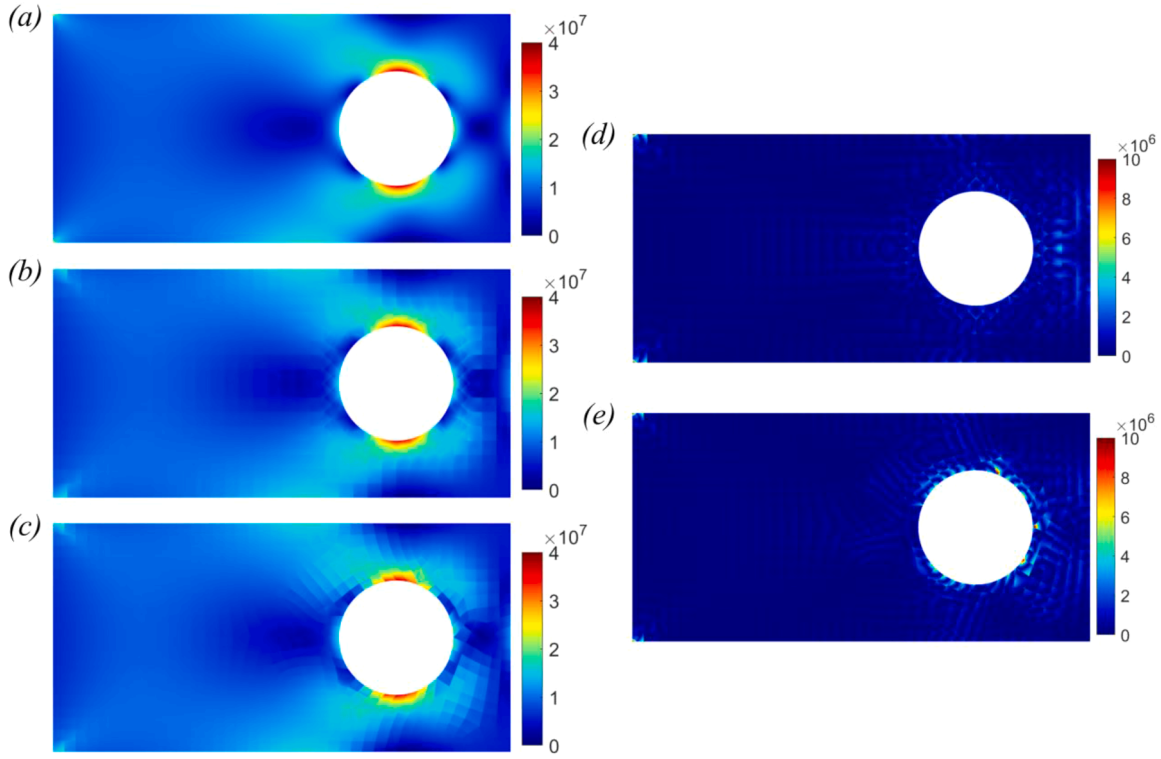

Fig. 11. Von Mises stress at 0.7 ms; (a) The reference solution; (b) Results using the AMORE mesh; (c) Results using the traditional mesh of the 4-node incompatible mode element; (d) Absolute error using the AMORE mesh; (e) Absolute error using the traditional mesh; all units in Pa.

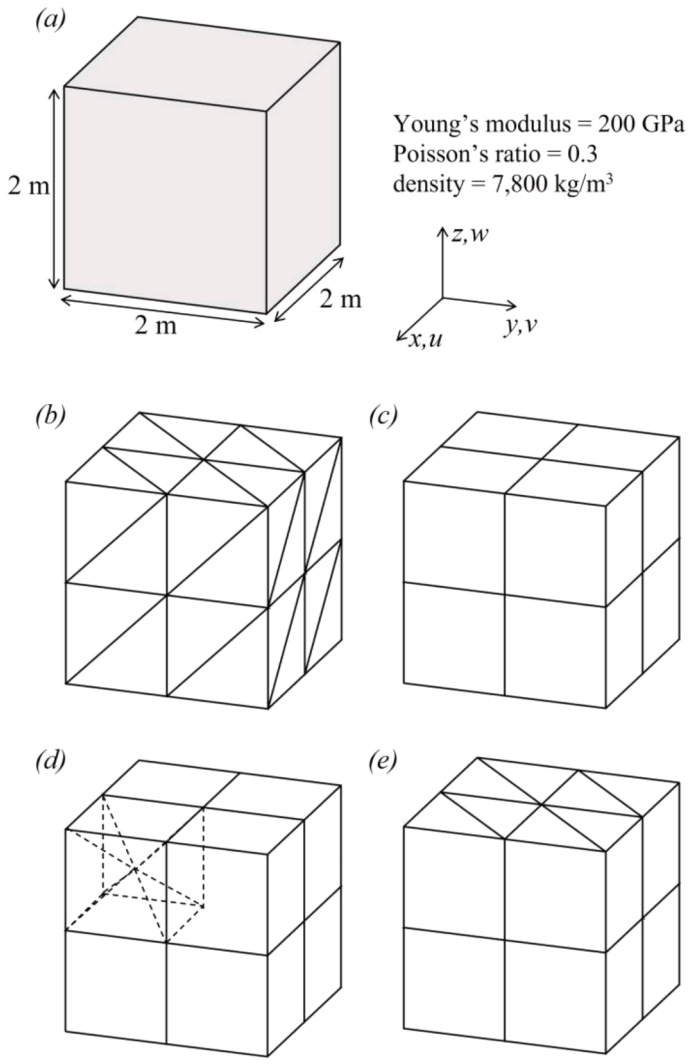

Fig. 12. Free vibration analysis of an unsupported cube; (a) Description of the analysis domain; (b) Mesh using tetrahedral elements; (c) using brick elements; (d) using pyramid elements; as shown, a set of six pyramid elements forms a sub-hexahedral domain; (e) Mesh using prism elements; all shown meshes correspond to $N = 2$ where N is the number of elements per side of the analysis domain; in the convergence studies, we use $N = 1$, 2, 4, and 8.

$$\begin{aligned} \mathbf{h}_K &= \rho_K \begin{bmatrix} 1 & \dfrac{(x - x_K)}{R_K} & \dfrac{(y - y_K)}{R_K} \end{bmatrix} \\ \mathbf{a}_K^u &= [\, a_{K1}^u \quad a_{K2}^u \quad a_{K3}^u \,] \\ \mathbf{a}_K^v &= [\, a_{K1}^v \quad a_{K2}^v \quad a_{K3}^v \,] \qquad \text{for } K = 1, 2, 3 \end{aligned} \tag{7}$$

where $(x_K, \quad y_K)$ are the Cartesian coordinates of node K, ρ_K was defined in Eq. (4), and R_K is the characteristic length associated with node K [9, 10].

Using the general principle of virtual work [1] and the displacement given by Eq. (5), we obtain for the overlapping finite element model without including a damping matrix

$$\mathbf{M}\ddot{\mathbf{U}} + \mathbf{K}\mathbf{U} = \mathbf{R} \tag{8}$$

where $\mathbf{M}$ is the global mass matrix, $\mathbf{K}$ is the global stiffness matrix, $\mathbf{U}$ is the unknown coefficient vector, and $\mathbf{R}$ is the external force vector. The global mass and stiffness matrices are assembled using the element mass and stiffness matrices

$$\begin{aligned} \mathbf{M} &= \sum_m \mathbf{M}^{(m)} = \sum_m \int_{V^{(m)}} \rho \mathbf{H}^{(m)T} \mathbf{H}^{(m)} dV^{(m)} \\ \mathbf{K} &= \sum_m \mathbf{K}^{(m)} = \sum_m \int_{V^{(m)}} \mathbf{B}^{(m)T} \mathbf{C} \mathbf{B}^{(m)} dV^{(m)} \end{aligned} \tag{9}$$

where ρ is the material density, $\mathbf{B}^{(m)}$ is the strain-displacement matrix, $\mathbf{C}$ is the material law matrix, and $V^{(m)}$ indicates the volume of element m.

In free vibration analysis, no external force is applied. Therefore, Eq. (8) becomes

$$\mathbf{M}\ddot{\mathbf{U}} + \mathbf{K}\mathbf{U} = \mathbf{0} \tag{10}$$

Assuming $\mathbf{U} = \mathbf{v}\sin \quad (\omega \quad t + t_0)$, we obtain the generalized eigenvalue problem

$$\mathbf{K}\mathbf{v} = \lambda \mathbf{M}\mathbf{v} \tag{11}$$

where $\lambda = \omega^2$, $\mathbf{K}$ contains no spurious mode and $\mathbf{M}$ is symmetric positive definite. Therefore, we have the eigenvalues and eigenvectors satisfying

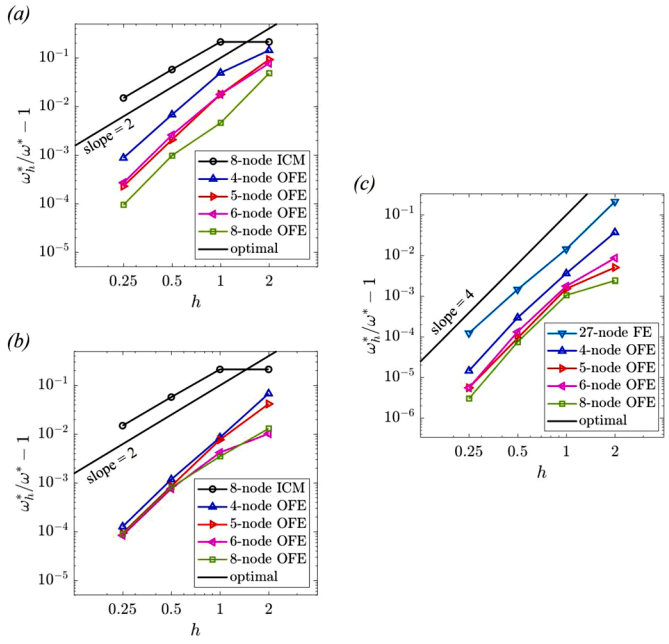

Fig. 13. Results of convergence studies using three-dimensional overlapping elements; (a) The use of linear basis; (b) bilinear basis; (c) quadratic basis; the ω_h^* and ω* indicate the numerical and reference solutions of the smallest nonzero frequency, respectively.

Table 3
Solution of cube for smallest 10 frequencies; solution times for obtaining the relative error less than 1% for the smallest frequency; the numerical and reference solutions of the frequency are denoted as ω_h^* and ω*, respectively; all times are normalized by the actual total CPU time of the 8-node incompatible mode element (ICM) solution.

Element (*N* of mesh)	$\log_{10}(\frac{\omega_h^*}{\omega^*}-1)$	Numerical integration time	Total CPU time	Half-bandwidth of **K**	Total degrees of freedom
8-node ICM (10)	−2.02	3.1×10^{-2}	1.0×10^{0}	996	3993
4-node linear OFE (4)	−2.17	1.2×10^{-2}	1.4×10^{-1}	264	1500
5-node linear OFE (3)	−2.27	1.0×10^{-2}	1.0×10^{-1}	642	1092
6-node linear OFE (3)	−2.22	4.7×10^{-3}	6.4×10^{-2}	276	768
8-node linear OFE (2)	−2.34	1.1×10^{-3}	2.0×10^{-2}	247	324

Table 4
Solution of cube for smallest 10 frequencies; solution times for obtaining the relative error less than 0.1% for the smallest nonzero frequency; the numerical and reference solutions of the frequency are denoted as ω_h^* and ω*, respectively; all times are normalized by the actual total CPU time of 8-node incompatible mode element (ICM) solution.

Element (*N* of mesh)	$\log_{10}(\frac{\omega_h^*}{\omega^*}-1)$	Numerical integration time	Total CPU time	Half-bandwidth of **K**	Total degrees of freedom
8-node ICM (32)	−3.02	1.7×10^{-3}	1.0×10^{0}	9510	107,811
4-node linear OFE (8)	−3.06	1.2×10^{-4}	5.1×10^{-3}	792	8748
5-node linear OFE (5)	−3.01	6.1×10^{-5}	2.2×10^{-3}	1644	4092
6-node linear OFE (6)	−3.13	5.4×10^{-5}	1.8×10^{-3}	852	4116
8-node linear OFE (4)	−3.01	1.9×10^{-5}	4.0×10^{-4}	744	1500

$$\begin{aligned}&\mathbf{K}\mathbf{v}_i=\lambda_i\mathbf{M}\mathbf{v}_i=\omega_i^2\mathbf{M}\mathbf{v}_i\\&0\le\lambda_1\le\lambda_2\le\ldots\le\lambda_n\\&\mathbf{v}_i^T\mathbf{K}\mathbf{v}_j=\delta_{ij}\lambda_i\\&\mathbf{v}_i^T\mathbf{M}\mathbf{v}_j=\delta_{ij}\end{aligned}\tag{12}$$

where n is the order of the square matrix **K**, ω_i and $\mathbf{v}_i$ are the i th natural frequency and corresponding mode shape, and δ_{ij} is the Kronecker delta.

In order to calculate the element stiffness and mass matrices, we use the numerical integration schemes given in Appendix A which are sufficiently high in order. With this numerical integration, we have that the resulting mass matrix is positive definite and the resulting stiffness matrix has no spurious zero energy mode.

Further, by the polynomial reproducibility of the overlapping finite element method and the approximation theory for the generalized eigenvalue problem [29,30], we have the following error estimate for the natural frequencies

$$|\omega_h-\omega|\le C\,h^{2p}\tag{13}$$

where ω_h and ω indicate the predicted and exact natural frequencies, respectively, h is the maximum overlapping element size, p is the order of the polynomial basis used, and C is a constant independent of h.

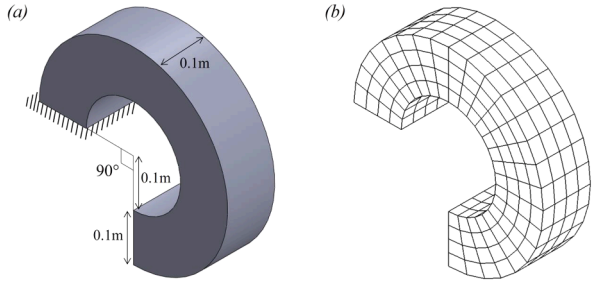

Fig. 14. (a) A three-dimensional slender ring; Young's modulus = 200 GPa, Poisson's ratio = 0.3, density = 7800 kg/m^3; (b) The mesh using $m = 4$.

Table 5
Solution of ring for smallest 20 frequencies; solution times for obtaining the relative error less than 1% for the smallest frequency; the numerical and reference solutions of the frequency are denoted as ω_h^* and ω^*, respectively; all times are normalized by the total CPU time used for the 8-node incompatible mode element (ICM) solution.

Element ($m \times m \times 6\,m$)	$\log_{10}(\frac{\omega_h^*}{\omega^*} - 1)$	Numerical integration time	Total CPU time	Half-bandwidth of **K**	Total degrees of freedom
8-node ICM ($8 \times 8 \times 48$)	−2.10	8.3×10^{-2}	1.0×10^{0}	705	11,664
8-node linear OFE ($4 \times 4 \times 24$)	−2.22	5.2×10^{-2}	7.6×10^{-1}	663	7275

Table 6
Solution of ring for smallest 20 frequencies; solution times for obtaining the relative error less than 0.1% for the smallest frequency; the numerical and reference solutions of the frequency are denoted as ω_h^* and ω^*, respectively; all times are normalized by the total CPU time used for the 8-node incompatible mode element (ICM) solution.

Element ($m \times m \times 6\,m$)	$\log_{10}(\frac{\omega_h^*}{\omega^*} - 1)$	Numerical integration time	Total CPU time	Half-bandwidth of **K**	Total degrees of freedom
8-node ICM ($24 \times 24 \times 144$)	−3.06	9.0×10^{-3}	1.0×10^{0}	5553	270,000
8-node linear OFE ($10 \times 10 \times 60$)	−3.07	3.1×10^{-3}	2.1×10^{-1}	3795	87,483

3.2. Mode superposition solution

The free vibration analysis provides frequencies and mode shapes to efficiently solve Eq. (8) when the external load has a limited frequency content. Suppose we have calculated p eigenvalues and corresponding eigenvectors. We use

$$\mathbf{U} = \widehat{\mathbf{V}}\mathbf{Q} \tag{14}$$

where $\widehat{\mathbf{V}} = \begin{bmatrix} \mathbf{v}_1 & \mathbf{v}_2 & \cdots & \mathbf{v}_p \end{bmatrix}$ is an $n \times p$ matrix of mode shapes and $\mathbf{Q} = \begin{bmatrix} q_1 & q_2 & \cdots & q_p \end{bmatrix}^T$ is a coefficient vector. Using Eq. (14), we transform Eq. (8) into

$$\widehat{\mathbf{V}}^T\mathbf{M}\widehat{\mathbf{V}}\ddot{\mathbf{Q}} + \widehat{\mathbf{V}}^T\mathbf{K}\widehat{\mathbf{V}}\mathbf{Q} = \widehat{\mathbf{V}}^T\mathbf{R} \tag{15}$$

and using the orthogonality of the eigenvectors in Eq. (12), we have

$$\ddot{\mathbf{Q}} + \widehat{\Lambda}\mathbf{Q} = \widehat{\mathbf{V}}^T\mathbf{R} \tag{16}$$

where $\widehat{\Lambda}$ is the diagonal matrix containing the eigenvalues

$$\widehat{\Lambda} = \begin{bmatrix} \lambda_1 & 0 & \cdots & 0 \\ 0 & \lambda_2 & & \vdots \\ \vdots & & \ddots & 0 \\ 0 & \cdots & 0 & \lambda_p \end{bmatrix} \tag{17}$$

In the mode superposition method, the time integration is performed for the p decoupled Eqs. (16), usually by a numerical integration which is inexpensive to perform [31]. Once **Q** has been solved for, we obtain the displacements using Eq. (14).

We see that the calculation of frequencies and mode shapes and the mode superposition solution are performed as in traditional finite element analysis [1] but considering that each node carries a polynomial as degrees of freedom. Hence the size n of the vector **U** in Eqs. (8) to (14) and of each mode shape $\mathbf{v}_i$ in Eqs. (14) to (16) now corresponds to the total number of unknowns in these polynomials.

4. Insight through numerical studies

We next provide numerical examples to obtain insight into the use of overlapping finite elements for the free vibration and mode superposition analyses. The convergence behavior and distortion sensitivity are numerically investigated, and we demonstrate the use of an AMORE mesh [2] in a mode superposition analysis. Of particular interest is the computational efficiency for three-dimensional solutions. For all computations, we used a laptop with a single core Intel 2.80 GHz CPU and 16 GB RAM.

4.1. Longitudinal vibration of a one-dimensional rod

We consider the free vibration behavior of the one-dimensional rod shown in Fig. 2. For this study we use the one-dimensional overlapping finite element with $\beta = 0.01$ and compare the results with those obtained using the corresponding traditional finite element, see Appendix B for the derivation of the interpolations of the overlapping element. We use a uniform mesh of ten elements. The calculated natural frequencies are plotted in Fig. 3 which shows that the overlapping finite element method provides accurate predictions of the frequencies, with the linear overlapping finite element giving accuracies similar to those obtained using

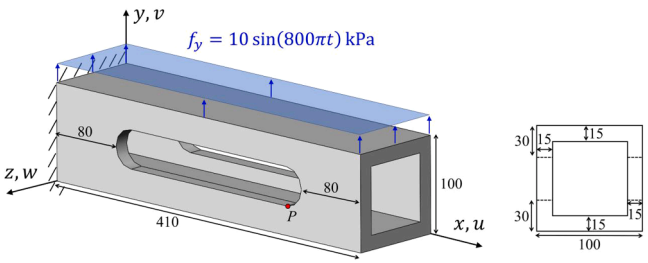

Fig. 15. Mode superposition analysis of a tool jig; Young's modulus = 200 GPa and Poisson's ratio = 0.3; the tool jig is subject to a sinusoidal *y*-direction surface traction; *t* denotes the time elapsed in seconds; lengths in mm.

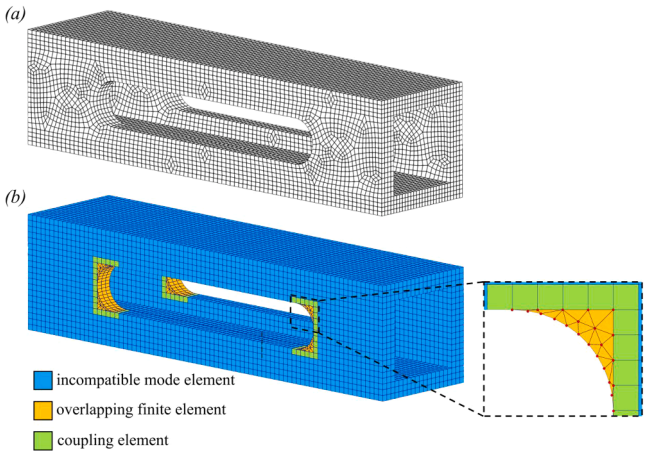

Fig. 16. (a) The traditional mesh using the incompatible mode element; (b) The AMORE mesh using the 6-node prism overlapping element [10] with the linear basis and β = 0.01; the 8-node coupling element is used; the red nodes in the zoomed image represent overlapping element nodes.

the 3-node quadratic finite element. For a given mesh, the overlapping finite element gives a larger number of natural frequencies because it uses nodal polynomials. The reference solution is the analytical solution.

If we use the quadratic overlapping element, the solution is composed of the constant, linear, quadratic terms with independent coefficients – i.e., the nodal polynomial at node *K* is

$$u_K = a_{K1} + a_{K2}\left(\frac{x - x_K}{R_K}\right) + a_{K3}\left(\frac{x - x_K}{R_K}\right)^2 \tag{18}$$

Fig. 4 shows the predicted second mode and the contribution of each term in the nodal polynomial. The linear and quadratic terms provide bubble-like displacements. In the traditional finite element solution the mode shape vector gives the displacements at the nodes which are interpolated between nodes; in the overlapping finite element method, all coefficients corresponding to the nodal polynomials give the displacements of the material particles. In this example, it is no surprise that the constant term used in the quadratic assumption gives already a quite accurate solution of the second mode shape, see Fig. 4, which corresponds to the results in Fig. 3.

4.2. Convergence of two-dimensional overlapping elements

To study the convergence properties of two-dimensional overlapping elements we solve for the in-plane vibrations of an unsupported plate with no displacement boundary conditions; hence, the first three smallest natural frequencies are zero, see Fig. 5. The behavior of the triangular and quadrilateral overlapping elements with β = 0.01 is investigated using the meshes described in Fig. 5(b) and (c). The smallest nonzero natural frequency is calculated and compared with the reference frequency obtained using a 50 × 50 mesh of 9-node finite elements. As can be seen in Fig. 6, both the triangular and quadrilateral overlapping elements show good convergence behavior. Note that for the same mesh the overlapping element provides better solution accuracy than the finite element counterpart.

4.3. Two-dimensional beam modeled with distorted elements

To investigate the distortion sensitivity of the overlapping elements, we solve for the smallest frequencies of a free-free beam using meshes with distorted elements, see Figs. 7 and 8.

Table 1 lists the results and includes also those using the incompatible mode (ICM) element and standard 9-node element. The reference frequencies are those obtained using a 100 × 20 mesh of 9-node finite elements. These results show a good distortion insensitivity of the overlapping elements.

4.4. Mode superposition solution of a plate

Here, we use the AMORE scheme for a mode superposition solution. Fig. 9 shows the structure considered, the loading and the meshes used. The overlapping elements in the AMORE mesh use the linear basis and β = 0.01. Considering that the excitation frequency = 2000 Hz and the fifth smallest natural frequency = 11,745 Hz, we employ the first five modes in the mode superposition method with the time step =5 μs. This time step is about one twentieth of the period of the highest frequency considered. To evaluate the solution accuracy, a comparison solution is calculated using the traditional mesh shown in Fig. 9(c). Both the AMORE and traditional meshes give a relative error of 0.2% (rounded) for the smallest natural frequency. The reference solution is calculated using a fine mesh of 9-node finite elements (39,038 dofs). The static correction [1] is performed in all solutions including the reference solution.

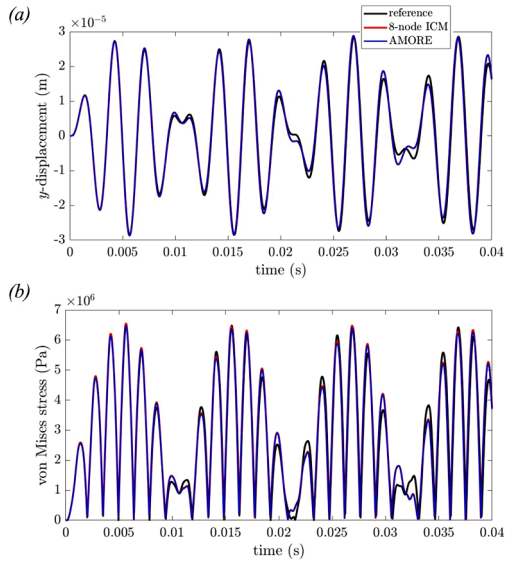

Fig. 17. Numerical predictions at point *P*, see Fig. 15; (a) the *y*-displacement; (b) the von Mises stress.

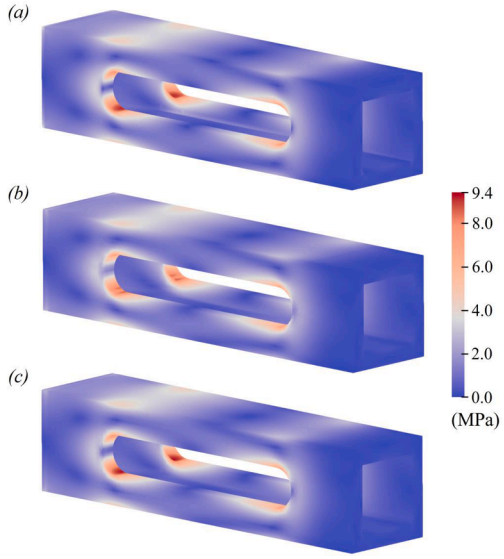

Fig. 18. von Mises stress prediction at $t = 0.027$ s; (a) Reference solution; (b) Solution obtained using the traditional mesh; (c) using the AMORE mesh.

As given in Table 2, the solution times are similar for the two solutions. However, we see in Figs. 10 and 11 that the AMORE mesh gives a more accurate stress prediction.

4.5. Convergence studies with three-dimensional overlapping elements

To study the convergence behavior in frequencies of the three-dimensional overlapping finite elements we consider the unsupported cube shown in Fig. 12. We use the tetrahedral, brick, pyramid, and prism overlapping elements in the meshes shown with the parameter *N*, and evaluate the ten lowest nonzero natural frequencies. Fig. 13 shows the relative error of the solution of the smallest frequency with respect to the element size used. All overlapping elements show good convergence behavior. The reference frequency is based on using the 27-node finite element in a uniform mesh of $32 \times 32 \times 32$ elements.

In Tables 3 and 4 we give the solution times for obtaining the ten smallest nonzero frequencies with the relative error of less than 1% and 0.1% for the smallest frequency. In the tables, the results for the linear overlapping element with $\beta = 0.01$ are compared with the use of the incompatible mode element. We see that in this analysis the use of the linear overlapping finite element method is much more efficient than using traditional finite elements.

4.6. Free vibration analysis of a three-dimensional ring

We further study the computational efficiency of the overlapping element method by considering the solution of the 20 smallest natural frequencies of the ring shown in Fig. 14, see Ref. [24]. We use the 8-node linear overlapping finite element with $\beta = 0.01$ and measure the solution times to reach the relative error for the smallest frequency less than 1% and 0.1%. Again, for comparison, we use the 8-node incompatible mode element solution. The meshes contain $m \times m \times 6\ m$ elements, with the larger number into the circumferential direction, see Fig. 14(b). A very fine mesh using 27-node elements (198,450 dofs) provides the reference solution. Tables 5 and 6 show that the use of the overlapping finite element method is quite efficient.

4.7. Forced vibration analysis of a three-dimensional tool jig

Finally, we consider the mode superposition solution of the bending problem given in Fig. 15. A mesh of 8-node incompatible mode elements (106,866 dofs) and an AMORE mesh (66,120 dofs) are used to solve the problem, see Fig. 16. We note that both meshes achieve the relative error of 0.3% for the smallest natural frequency. The solution using a fine 27-node element mesh (867,258 dofs) is the reference solution.

The ten smallest frequencies are sought in the subspace iteration solution, and among them the six smallest frequencies and associated modes are employed for the modal superposition solution. Note that the sixth smallest frequency is about four times the excitation frequency (i.e., 400 Hz). For all solutions, the time step is 30 μs which is about one twentieth of the period of the sixth mode and the static correction is applied.

We see that the use of the AMORE and traditional meshes results in similar solution accuracies for numerical predictions at point *P* (see Figs. 15 and 17) while the CPU time is less when using the AMORE mesh (see Table 7). Fig. 18 shows the predicted von Mises stress distributions at $t = 0.027$ s.

5. Concluding remarks

Our objective in this paper was to study the use of the recently developed 'overlapping finite elements' in the solution of frequencies and mode shapes and in the method of superposition. The fundamental equations used were given followed by focusing on the computational efficiency of the overlapping finite elements when compared to the use of traditional finite elements. For the frequencies and mode shape solutions, the Bathe subspace iteration method was used.

The paper shows that in essence all methods available for the

Table 7
Solution of tool jig for smallest 10 frequencies; all times are normalized by the actual total CPU time used for the 8-node incompatible mode element (ICM) solution; note that both meshes give the relative error of 0.3% for the first frequency.

Mesh	Numerical integration time	Time for time integration	Total CPU time	Half-bandwidth of **K**	Total degrees of freedom
AMORE	1.6×10^{-2}	4.2×10^{-3}	3.5×10^{-1}	1995	66,120
8-node ICM	2.0×10^{-2}	5.4×10^{-3}	1.0×10^{0}	2577	106,866

traditional finite element method can be directly extended for use with overlapping elements and these extensions are not difficult to accomplish. The solutions of two- and three-dimensional problems using all the developed overlapping elements (including prism and pyramid elements) indicated that the overlapping elements could be used effectively for dynamic analyses, but of course only some problems were considered. We also solved for transient response using AMORE meshes which indicated that for transient analyses the use of AMORE can also be effective.

However, in all solutions the computational schemes employed were not optimized with respect to computational times, in particular the solution of the equations in the subspace iteration scheme need optimization, like the use of modern sparse solvers. It may well be that such optimization would be of particular value for the overlapping finite element discretizations and the use of AMORE.

Finally, while we see great potential in the use of overlapping finite elements and AMORE, we also are aware that much further research is needed to fully develop this novel approach. The solution schemes need to be studied, extended and improved for general nonlinear analyses and for the solution of multiphysics problems. Also, model order reduction techniques may be effective in this approach, in particular for special applications like fracture [32]. In all these endeavors the automatic meshing for optimal efficiency needs particular attention.

Declaration of Competing Interest

The authors declare that they have no known competing financial interests or personal relationships that could have appeared to influence the work reported in this paper.

Appendix A Numerical integration schemes used for overlapping finite elements

We give here the numerical integration schemes we used for overlapping elements. For the calculation of the stiffness matrix, we use the rules given in Table A1. With these rules, the elements are complete and exhibit no spurious mode. The mass matrix is obtained using the rules in Table A2 which render the mass matrix positive definite. The label GQ denotes the use of the Gaussian quadrature, and we give the references.

Table A1
Numerical integration rules used for evaluating the element stiffness matrix of overlapping element; the first, second, and third columns are for using the linear, bilinear, and quadratic bases, respectively.

4-node quadrilateral	GQ 3×3	GQ 4×4	GQ 5×5
3-node triangular	6 [33]	9 [33]	16 [34]
4-node tetrahedral	11 [35]	24 [35]	46 [34]
8-node brick	GQ $3 \times 3 \times 3$	GQ $4 \times 4 \times 4$	GQ $5 \times 5 \times 5$
6-node prism	r- and s-directions: 6 [33]	r- and s-directions: 9 [33]	r- and s-directions: 16 [34]
	t-direction: GQ 3	t-direction: GQ 4	t-direction: GQ 4
5-node pyramid	t-direction: GQ 3	t-direction: GQ 4	t-direction: GQ 5
	GQ 3×3 on $t = -0.774597$	GQ 4×4 on $t = -0.861136$	GQ 4×4 on $t = -0.906180$
	GQ 2×2 on $t = 0.000000$	GQ 3×3 on $t = -0.339981$	GQ 4×4 on $t = -0.538469$
	GQ 1×1 on $t = 0.774597$	GQ 2×2 on $t = 0.339981$	GQ 3×3 on $t = 0.000000$
		GQ 1×1 on $t = 0.861136$	GQ 2×2 on $t = 0.538469$
			GQ 1×1 on $t = 0.906180$

Table A2
Numerical integration rules used for evaluating the element mass matrix of overlapping elements; the first, second, and third columns are for using the linear, bilinear, and quadratic bases, respectively.

4-node quadrilateral	GQ 4×4	GQ 4×4	GQ 6×6
3-node triangular	9 [33]	16 [34]	28 [36]
4-node tetrahedral	17 [37]	46 [34]	236 [34]
8-node brick	GQ $4 \times 4 \times 4$	GQ $4 \times 4 \times 4$	GQ $6 \times 6 \times 6$
6-node prism	r- and s-directions: 9 [33]	r- and s-directions: 12 [33]	r- and s-directions: 28 [36]
	t-direction: GQ 4	t-direction: GQ 4	t-direction: GQ 5
5-node pyramid	t-direction: GQ 3	t-direction: GQ 4	t-direction: GQ 5
	GQ 4×4 on $t = -0.774597$	GQ 4×4 on $t = -0.861136$	GQ 5×5 on $t = -0.906180$
	GQ 2×2 on $t = 0.000000$	GQ 4×4 on $t = -0.339981$	GQ 4×4 on $t = -0.538469$
	GQ 1×1 on $t = 0.774597$	GQ 2×2 on $t = 0.339981$	GQ 4×4 on $t = 0.000000$
		GQ 1×1 on $t = 0.861136$	GQ 2×2 on $t = 0.538469$
			GQ 1×1 on $t = 0.906180$

Appendix B Formulation of the one-dimensional overlapping element

The one-dimensional overlapping element uses the following ϕ_K^I

$$\phi_K^I = \widehat{h}_1\widehat{\phi}_{K1}^I + \widehat{h}_2\widehat{\phi}_{K2}^I + \widehat{h}_3\widehat{\phi}_{K3}^I \tag{B.1}$$

where the $\widehat{\phi}_{Ki}^I$ are defined in Table B1 and the $\widehat{h}_i$ are the 3-node finite element functions

$$\begin{aligned}\widehat{h}_1 &= (1-r)/2 - 0.5\widehat{h}_3\\ \widehat{h}_2 &= (1+r)/2 - 0.5\widehat{h}_3\\ \widehat{h}_3 &= \left(1-r^2\right)\end{aligned} \tag{B.2}$$

for which the node numbering is shown in Fig. B1.

Therefore, by Eqs. (1) and (2), we have

$$\begin{aligned}u^{(m)} &= h_1\left(\phi_1^1u_1 + \phi_2^1u_2\right) + h_2\left(\phi_1^2u_1 + \phi_2^2u_2\right)\\ &= \left(h_1\phi_1^1 + h_2\phi_1^2\right)u_1 + \left(h_1\phi_2^1 + h_2\phi_2^2\right)u_2\\ &= \rho_1u_1 + \rho_2u_2\end{aligned} \tag{B.3}$$

where $\rho_1 = h_1 + \beta(h_2 - h_1)\widehat{h}_3$ and $\rho_2 = h_2 + \beta(h_1 - h_2)\widehat{h}_3$ following Eq. (4).

Table B1
Nodal values for the interpolation of ϕ_K^I of the 2-node overlapping elements.

Nodes	$i=1$	2	3
$\widehat{\phi}_{1i}^1$	1	0	$0.5-\beta$
$\widehat{\phi}_{2i}^1$	0	1	$0.5+\beta$
$\widehat{\phi}_{1i}^2$	1	0	$0.5+\beta$
$\widehat{\phi}_{2i}^2$	0	1	$0.5-\beta$

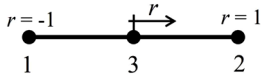

Fig. B1. The node numbering for the one-dimensional overlapping finite element.

References

[1] Bathe KJ. Finite element procedures. Prentice Hall; 1996. 2nd ed. KJ Bathe, Watertown, MA; 2014, and Higher Education Press, Beijing; 2016.
[2] Bathe KJ. The AMORE paradigm for finite element analysis. Adv Eng Softw 2019; 130:1–13.
[3] Payen DJ, Bathe KJ. A stress improvement procedure. Comput Struct 2012;112-113:311–26.
[4] Lee NS, Bathe KJ. Effects of element distortions on the performance of isoparametric elements. Int J Numer Methods Eng 1993;36:3553–76.
[5] Bathe KJ, Zhang L. The finite element method with overlapping elements–a new paradigm for CAD driven simulations. Comput Struct 2017;182:526–39.
[6] Zhang L, Bathe KJ. Overlapping finite elements for a new paradigm of solution. Comput Struct 2017;187:64–76.
[7] Zhang L, Kim KT, Bathe KJ. The new paradigm of finite element solutions with overlapping elements in CAD – computational efficiency of the procedure. Comput Struct 2018;199:1–17.
[8] Huang J, Bathe KJ. Quadrilateral overlapping elements and their use in the AMORE paradigm. Comput Struct 2019;222:25–35.
[9] Lee S, Bathe KJ. An enhancement of overlapping finite elements. Comput Struct 2022;260:106704.
[10] Lee S, Bathe KJ. Additional overlapping finite elements – the pyramid and prism elements. Comput Struct 2022;268:106813.
[11] Kim KT, Zhang L, Bathe KJ. Transient implicit wave propagation dynamics with overlapping finite elements. Comput Struct 2018;199:18–33.
[12] Chai Y, Bathe KJ. Transient wave propagation in inhomogeneous media with enriched overlapping triangular elements. Comput Struct 2020;237:106273.
[13] Kim KT, Bathe KJ. Accurate solution of wave propagation problems in elasticity. Comput Struct 2021;249:106502.
[14] Strouboulis T, Babuška I, Copps K. The design and analysis of the generalized finite element method. Comput Methods Appl Mech Eng 2000;181:43–69.
[15] Duarte CA, Babuška I, Oden JT. Generalized finite element methods for three-dimensional structural mechanics problems. Comput Struct 2000;77:215–32.
[16] Babuška I, Banerjee U. Stable generalized finite element method (SGFEM). Comput Methods Appl Mech Eng 2012;201-204:91–111.
[17] Zhang Q, Banerjee U, Babuška I. Higher-order stable generalized finite element method. Numer Math 2014;128:1–29.
[18] Sato FM, Piedade Neto D, Proença SPB. Numerical experiments with the generalized finite element method based on a flat-top partition of unity. Lat Am J Solids Struct 2018;15(11) [online].
[19] Kim S, Lee PS. A new enriched 4-node 2D solid finite element free from the linear dependence problem. Comput Struct 2018;202:25–43.
[20] Kim S, Lee PS. New enriched 3D solid finite elements: 8-node hexahedral, 6-node prismatic, and 5-node pyramidal elements. Comput Struct 2019;216:40–63.
[21] Bachene M, Tiberkak R, Rechak S. Vibration analysis of cracked plates using the extended finite element method. Arch Appl Mech 2009;79:249–62.
[22] Arndt M, Machado RD, Scremin A. An adaptive generalized finite element method applied to free vibration analysis of straight bars and trusses. J Sound Vib 2010; 329:659–72.
[23] da Silva IA, Machado RD, Arndt M, de Oliveira Weinhardt P. Assessment of the flat-top stable GFEM for free vibration analysis. Comput Math with Appl 2022;117: 271–83.
[24] Kim KT, Bathe KJ. The Bathe subspace iteration method enriched by turning vectors. Comput Struct 2017;186:11–21.
[25] Kim K-T, Bathe KJ., Implementation of the enriched subspace iteration method 2017. http://meche.mit.edu/people/faculty/kjb%40mit.edu (accessed May 31, 2022).
[26] George A, Liu J.W. Computer solution of large sparse positive definite. Prentice Hall Professional Technical Reference; 1981.
[27] De S, Bathe KJ. The method of finite spheres. Comput Mech 2000;25:329–45.

[28] Kim J, Bathe KJ. The finite element method enriched by interpolation covers. Comput Struct 2013;116:35–49.
[29] Babuška I., Osborn J. Eigenvalue problems. In: Ciarlet PG, Lions JL. editors. Handbook of numerical analysis, Vol. II, Amsterdam; 1991, p. 641–787.
[30] Huang J, Bathe KJ. On the convergence of overlapping elements and overlapping meshes. Comput Struct 2021;244:106429.
[31] Bathe KJ, Noh G. Insight into an implicit time integration scheme for structural dynamics. Comput Sturct 2012;98-99:1–6.
[32] Kerfriden P, Goury O, Rabczuk T, Bordas SPA. A partitioned model order reduction approach to rationalise computational expenses in nonlinear fracture mechanics. Comput Methods Appl Mech Eng 2013;256:169–88.
[33] Cowper GR. Gaussian quadrature formulas for triangles. Int J Numer Methods Eng 1973;7:405–8.
[34] Zhang L, Cui T, Liu H. A set of symmetric quadrature rules on triangles and tetrahedra. J Comput Math 2009;27:89–96.
[35] Keast P. Moderate-degree tetrahedral quadrature formulas. Comput Methods Appl Mech Eng 1986;55:339–48.
[36] Lyness JN, Jespersen D. Moderate degree symmetric quadrature rules for the triangle. IMA J Appl Math 1975;15:19–32.
[37] Yu J. Symmetric Gaussian quadrature formulae for tetrahedronal regions. Comput Methods Appl Mech Eng 1984;43:349–53.